ATLAS NOTE

ATLAS-CONF-2013-020

March 6, 2013

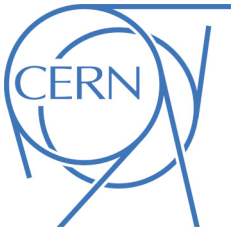

Measurement of the total ZZ production cross section in proton-proton collisions at $\sqrt{s}$ = 8 TeV in 20 fb^{-1} with the ATLAS detector

ATLAS Collaboration

Abstract

The ZZ production cross section has been measured by the ATLAS experiment using the four-lepton decay channel, where the term lepton implies electrons and muons. A data sample of 20.3±0.6 fb^{-1} collected in pp collisions at $\sqrt{s}$ = 8 TeV at the LHC in 2012 is used. Events are selected by requiring four leptons, forming two opposite-sign same-flavour lepton pairs each with an invariant mass between 66 GeV and 116 GeV. We observe 305 candidate events with a background expectation of 20.4±2.9(stat)±5.0(syst.). The $ZZ \to \ell^-\ell^+\ell'^-\ell'^+$ production cross section is measured to be $20.7^{+1.3}_{-1.2}$(stat.) ± 0.8(syst.) ± 0.6(lumi.) fb in a fiducial phase-space corresponding closely to the acceptance region. After correcting for the $ZZ \to \ell^-\ell^+\ell'^-\ell'^+$ branching fraction and the fiducial acceptance, the total ZZ production cross section is measured to be $7.1^{+0.5}_{-0.4}$(stat.)±0.3(syst.)±0.2(lumi.) pb, where the total cross section is defined by requiring both Z bosons to have an invariant mass between 66 GeV and 116 GeV. This result is consistent with the Standard Model expectation of $7.2^{+0.3}_{-0.2}$ pb.

ATLAS-CONF-2013-020
08 March 2013

1 Introduction

The production of Z-boson pairs at the Large Hadron Collider (LHC) is of great interest since it provides an excellent opportunity to test the predictions of the electroweak sector of the Standard Model (SM) at the TeV energy scale. Deviations from SM expectations for the total or differential ZZ production cross sections could be indicative of the production of new resonances decaying to Z bosons or other non-SM contributions.

In the Standard Model, ZZ production proceeds via quark-antiquark t-channel annihilation, with a small contribution from gluon fusion, calculated using MCFM [1] to be 5.9% in pp collisions at 8 TeV. Figure 1 shows the corresponding Feynman diagrams for ZZ production. The ZZZ and $ZZ\gamma$ neutral triple gauge boson couplings (nTGCs) are zero in the Standard Model, hence there is no contribution from s-channel $q\bar{q}$ annihilation at tree level. At the one-loop level, the contribution is $O(10^{-4})$ [2]. Many models of physics beyond the Standard Model predict values of nTGCs at the level of 10^{-4} to 10^{-3} [3]. Those non-zero nTGCs can increase the ZZ cross section especially for high ZZ invariant mass and high transverse momentum of the Z bosons [4].

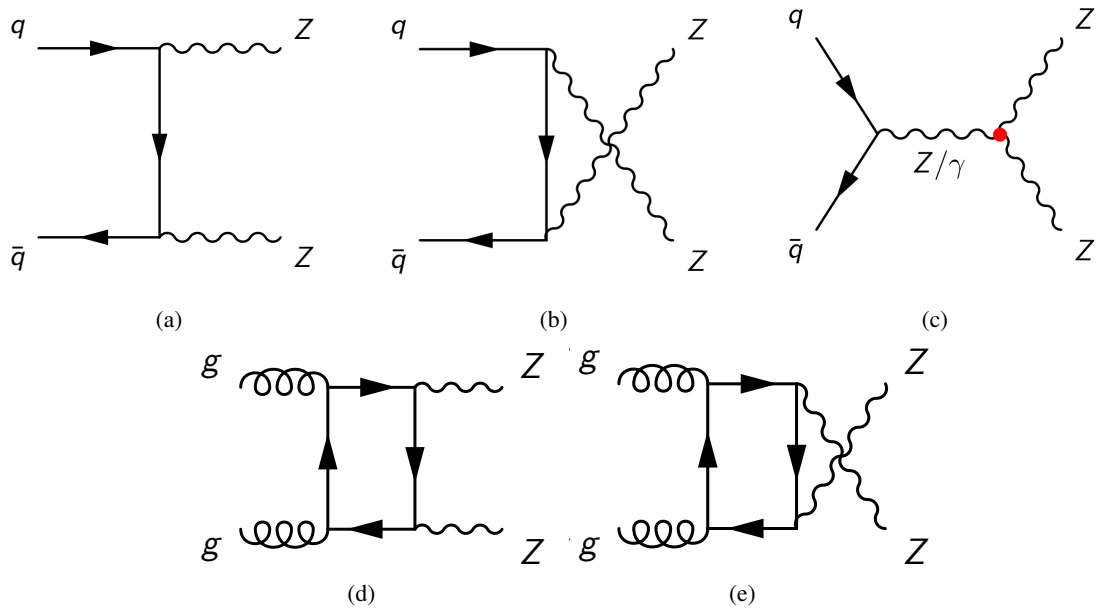

Figure 1: Leading order Feynman diagrams for ZZ production through the $q\bar{q}$ and gg initial state at hadron colliders. The s-channel diagram, (c), contains the ZZZ and $ZZ\gamma$ neutral TGC vertices which do not exist in the SM.

Recently, the ATLAS [5] and CMS [6] collaborations have measured the ZZ production cross section in proton-proton collisions at $\sqrt{s} = 7$ TeV. There are also results from ATLAS [7] and CMS [8] at a centre-of-mass energy of $\sqrt{s} = 8$ TeV using part of the data collected during 2012. The results shown here supercede the previous ATLAS result at $\sqrt{s} = 8$ TeV. ZZ production has also been studied in e^+e^- collisions at LEP [9–13] and in proton-antiproton collisions at the Tevatron [14, 15]. No deviation of the measured cross section from the Standard Model expectation has been observed, allowing limits on non-zero (anomalous) nTGCs to be set. The production cross section at the LHC for a centre-of-mass energy of 8 TeV is predicted to be about 5.5 times larger than at the Tevatron, and about 1.2 times larger than in 7 TeV collisions at the LHC.

In this note we present the measurement of the cross section for ZZ production (throughout this note

Z should be taken to mean Z/γ^*) in proton-proton collisions at a centre-of-mass energy of 8 TeV, using a data sample corresponding to an integrated luminosity of 20.3±0.6 fb^{-1} collected by the ATLAS detector at the LHC during 2012. The cross section for ZZ production, requiring both Z bosons to have masses between 66 GeV and 116 GeV, calculated at next-to-leading order (NLO) in QCD using MCFM with the CT10 [16] NLO parton distribution function (PDF) set and using the natural width of the Z boson, is found to be $7.2^{+0.3}_{-0.2}$ pb. The quoted theoretical uncertainties result from varying the factorization and renormalization scales (which are by default equal to half the mass of the diboson system) simultaneously by a factor of two whilst using the full CT10 PDF error set. The cross section calculated using the on-shell (zero-width) approximation is 5% higher.

Candidate ZZ events are reconstructed in the $ZZ \to \ell^-\ell^+\ell'^-\ell'^+$ decay channel, where ℓ can be an electron or a muon. Although this channel constitutes only 0.45% of the total ZZ cross section, its branching fractions are known precisely and the experimental signature of four high transverse-momentum isolated leptons is very distinctive and benefits from extremely small backgrounds.

We first measure the cross section in a fiducial phase-space that closely matches the experimental acceptance, thus reducing the theory-dependent systematic uncertainties of the measurement; we refer to this as the 'fiducial cross section'. A fiducial phase-space common to all three decay channels ($e^+e^-e^+e^-$, $\mu^+\mu^-\mu^+\mu^-$ and $e^+e^-\mu^+\mu^-$) is defined by requiring four leptons to be within the pseudorapidity range[1] $|\eta| < 2.7$, to have transverse momentum (p_{T}) greater than 7 GeV, and to have $\Delta R \equiv \sqrt{\Delta\phi^2 + \Delta\eta^2} > 0.2$ for any two leptons. The invariant mass of both opposite-sign same-flavour lepton pairs is required to be between 66 and 116 GeV. The fiducial cross section is obtained from the reconstructed number of events (after background subtraction) using a reconstruction correction factor given by the number of simulated ZZ events which satisfy the full event selection divided by the number of ZZ events generated in the fiducial region (C_{ZZ}). The reconstruction acceptance factors are different for each of the three decay channels, reflecting not only the different efficiencies, but also the slightly different event selections amongst the three channels. In calculating the invariant masses of the lepton pairs at generator level, photons within $\Delta R = 0.1$ of a lepton are included in the lepton four-momentum to minimize the dependence on the generator modelling of collinear radiation.

The total ZZ cross section is calculated using the ZZ fiducial cross section, the $Z \to \ell^+\ell^-$ branching ratio [17], and a fiducial acceptance factor (A_{ZZ}) which is given by the fraction of ZZ events with Z bosons in the Z mass window that fall into the fiducial region. The fiducial acceptance factor A_{ZZ} is calculated from the NLO Standard Model prediction using MCFM. The total cross section is defined with both Z bosons having masses between 66 GeV and 116 GeV.

The main background arises from Z+jets events, from other diboson ($W^+W^-/W^\pm Z$) final states and from top-quark events ($t\bar{t}$ and single top) where the $t \to Wb$ decay is followed by a leptonic W boson decay and a semi-leptonic b-quark decay. Additional backgrounds arise from the irreducible sources $t\bar{t}Z$ and ZZZ/ZWW, which can produce four leptons. The background from $ZZ \to \ell^+\ell^-\tau^+\tau^-$ and $ZZ \to \tau^+\tau^-\tau^+\tau^-$, where the τ leptons decay to electrons or muons, is estimated from simulation to contribute 0.30% ± 0.02% of selected ZZ events after applying the full event selection described below. We correct for this contamination in the reconstruction acceptance factor defined above, which translates from the reconstructed event count to the number of true $ZZ \to \ell^-\ell^+\ell'^-\ell'^+$ decays within the fiducial phase-space.

The ATLAS detector has been described in detail elsewhere [18]. Since we only use electrons and muons in this measurement, the important components for this analysis are the inner tracking detector, the electromagnetic calorimeter and the muon spectrometer.

This note is organized as follows. Section 2 briefly describes the data sample used in this analysis and

[1] ATLAS uses a right-handed coordinate system with its origin at the nominal interaction point in the centre of the detector and the z-axis along the beam direction. The x-axis points from the interaction point to the centre of the LHC ring, and the y-axis points upwards. Cylindrical coordinates (r,ϕ) are used in the transverse plane, ϕ being the azimuthal angle around the beam direction. The pseudorapidity η is defined in terms of the polar angle θ as $\eta = -\ln\tan(\theta/2)$.

the Monte Carlo simulation used to estimate the signal expectation and to cross-check the background estimation. The event selection and signal efficiency are discussed in Section 3, details on the signal acceptance are given in Section 4 and the background estimation is described in Section 5. The cross section results are presented in Section 6. Conclusions are given in Section 7.

2 Dataset and Monte Carlo Simulation

Events were selected using single-lepton triggers with thresholds on the transverse momentum of the triggering lepton of 24 GeV both for electrons and muons. Data flagged with quality problems that affect the lepton reconstruction are removed. After data quality cuts, the total integrated luminosity used in the analysis is 20.3 ± 0.6 fb^{-1}. The uncertainty on the integrated luminosity is $\pm 2.8\%$. It is derived, following the same methodology as that detailed in Ref. [19], from a preliminary calibration of the luminosity scale derived from beam-separation scans performed in November 2012.

The reconstruction correction factors are determined from a detailed Monte Carlo simulation. The NLO generator PowhegBox [20–23] with NLO PDF set CT10 is used to model $qq \to ZZ \to \ell^+\ell^-\ell'^+\ell'^-$ events, where ℓ includes electrons, muons and τ leptons. The PowhegBox calculation does not include the next-to-next-to-leading order (NNLO) gluon-gluon diagrams. We simulate this contribution to the cross section using the gg2zz [24] generator, also using the CT10 PDF set. The simulations include the interference terms between the Z and γ^* diagrams.

The contributions from background processes are estimated from the data and are validated with predictions from Monte Carlo simulations. MC@NLO [25] is used to model $t\bar{t}$ and single top-quark events, and MadGraph [26] is used for the $t\bar{t} + W^{\pm}/Z$, ZZZ and ZWW final states. $W^{\pm}$ or Z bosons produced in association with jets, as well as the the diboson processes W^+W^- and $W^{\pm}Z$, are simulated with PowhegBox. Events with heavy flavour dijets are modelled with PythiaB [27]. The underlying event, parton shower, hadronization and τ lepton decays in the PowhegBox and MadGraph samples are modelled using Pythia 8 [28]. The underlying event in gg2zz and MC@NLO samples is modelled using Jimmy [29], while the parton shower and hadronization are modelled using Herwig [30], and the τ lepton decays are modelled using Tauola [31]. In all samples, the final-state radiation of photons is modelled using Photos [32].

The detector response is simulated [33] with a program based on GEANT4 [34]. The mean number of pp collisions per bunch crossing (referred to as 'pile-up') is between 5 and 40 for the 2012 data considered in this analysis. Additional inelastic pp events are included in the simulation, and the generated events are re-weighted so as to reproduce the observed distribution of average number of collisions per bunch-crossing in the data. An additional contribution to the pile-up comes from the ongoing detector response to interactions in the preceding bunch crossings; this is also modelled in the simulation.

3 Event Selection

Signal events are characterized by four high-p_{T}, isolated electrons or muons. To ensure that they originate from the primary vertex, lepton candidates are required to have the absolute value of the product of the longitudinal impact parameter (distance of closest approach) with respect to the primary vertex times the sine of the polar angle θ to be less than 0.5 mm. The primary vertex is defined as the vertex whose constituent tracks have the largest sum of p_{T}^2. To reject heavy flavour background, muons must have an impact parameter significance (the transverse impact parameter, d_0, divided by its error) less than 3 while the electrons must have an impact parameter significance less than 6.

Muons are identified by tracks (or track segments) reconstructed in the muon spectrometer matched to tracks reconstructed in the inner detector, and are required to have $p_{\mathrm{T}} > 7$ GeV and $|\eta| < 2.5$.

Their momentum is calculated by statistically combining the information from the two subsystems and correcting for parameterized energy loss in the calorimeter. In order to reject muons from the decay of heavy quarks, it is required that isolated muons be selected by restricting the scalar sum of the transverse momenta ($\sum p_{\mathrm{T}}$) of other tracks inside a cone of $\Delta R = 0.2$ around the muon to be no more than 15% of the muon p_{T}.

In the region $|\eta| < 0.1$ (where there is a limited geometric coverage in the muon spectrometer) calorimeter-tagged muons are considered in addition. They are reconstructed from calorimeter energy deposits consistent with a muon which are matched to an inner detector track with $p_{\mathrm{T}} > 20$ GeV and are required to satisfy the same impact parameter and isolation criteria as for the combined muons. Muons with $2.5 < |\eta| < 2.7$ (in a region outside the nominal coverage of the inner detector) are taken into account as well. They are required to have a full track that is reconstructed in the muon spectrometer. If these forward spectrometer muons are also measured in the inner detector, their momentum is measured using the combined information; otherwise, only the muon spectrometer information is used. In either case, such muons are required to have $p_{\mathrm{T}} > 10$ GeV. Instead of the above-mentioned $\sum p_{\mathrm{T}}$ isolation criteria, the $\sum E_{\mathrm{T}}$ of calorimeter energy deposits inside a cone of size $\Delta R = 0.2$ around these muons is required to be no more than 15% of their p_{T}. The same impact parameter requirements as for the muons with $|\eta| < 2.5$ are imposed for the forward muons measured in the inner detector; no such requirement is imposed on those measured in the muon spectrometer only. The number of calorimeter-tagged muons and muons with $2.5 < |\eta| < 2.7$ per event is limited to a maximum of one per type and it is also required that they be paired with muons which are neither calorimeter-tagged nor in the forward region, $2.5 < |\eta| < 2.7$. The inclusion of these two types of muons increases the expected event yield by 10%.

Electrons are reconstructed from energy deposits in the electromagnetic calorimeter matched to a track in the inner detector. For the 2012 LHC data taking, the electron reconstruction algorithm has been improved with respect to 2011. The ATLAS track pattern recognition and global χ^2 fit were modified to account for energy losses. Candidate electrons were fitted using a Gaussian-sum filter [35, 36] to account for bremsstrahlung energy losses. The track-to-cluster matching algorithm was then modified to benefit from these improvements. Electron candidates are required to have $p_{\mathrm{T}} > 7$ GeV and $|\eta| < 2.47$. They must be isolated, using the same criteria as for muons within $|\eta| = 2.5$, but calculating $\sum p_{\mathrm{T}}$ around the electron track. Electron candidates within $\Delta R = 0.1$ of any selected muon are rejected, and if two electron candidates overlap within $\Delta R = 0.1$ the electron with the lower p_{T} is rejected. The electron identification algorithm was chosen to maximimize efficiency at the cost of electron-like jet rejection and is relaxed compared to the identification algorithm used in the ATLAS $H \to ZZ^* \to \ell^+\ell^-\ell'^+\ell'^-$ analysis [37].

Events are required to have exactly four leptons selected as above, and to have passed a single-muon or single-electron trigger. To ensure that selected events have well measured trigger efficiency, at least one of these leptons must have $p_{\mathrm{T}} > 25$ GeV and match to a muon or electron reconstructed by the trigger algorithm with $\Delta R < 0.1$ for a muon or $\Delta R < 0.15$ for an electron. The matched lepton must be within the triggerable η volume ($|\eta| < 2.5$ for electrons and $|\eta| < 2.4$ for muons) and pass more stringent identification requirements than those in the trigger. The efficiency for triggering an event passing all of the other selection requirements is 99.0±0.1%, estimated using signal Monte Carlo simulation corrected by scale factors measured in data using a large number of dilepton events.

Same-flavour, oppositely-charged lepton pairs are combined to form Z candidates. An event must contain two such pairs. In the $e^+e^-e^+e^-$ and $\mu^+\mu^-\mu^+\mu^-$ final states there is an ambiguity in pairing the leptons into Z bosons. It is resolved by choosing the pairing which results in the smaller value of the sum of the two $|m_{\ell^+\ell^-} - m_Z|$ values, where $m_{\ell^+\ell^-}$ is the invariant mass of a lepton pair and m_Z is the mass of the Z boson [17]. However, if any same-flavour, oppositely-charged lepton pairing results in an invariant mass below 5 GeV, the event is rejected to reduce backgrounds including J/ψ mesons. Figure 2 shows a scatter plot of the invariant mass of the leading (higher p_{T}) lepton pair against that of the subleading

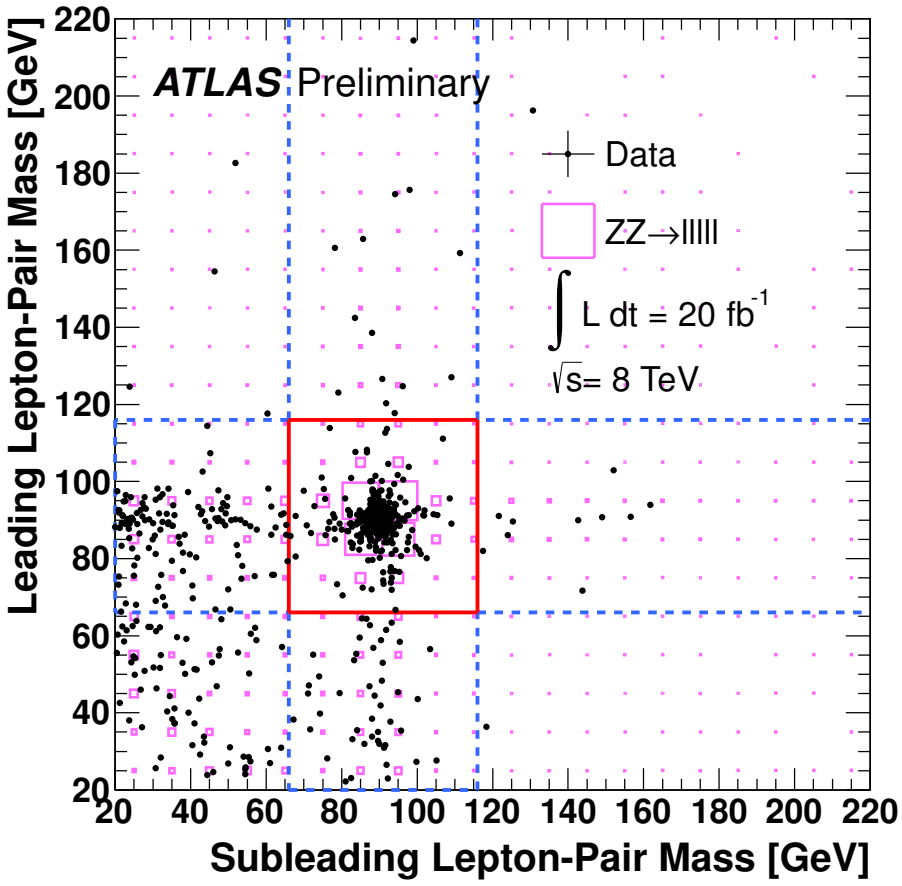

Figure 2: Invariant mass of the leading Z candidate versus the invariant mass of the subleading Z candidate. The events observed in the data are shown as solid circles and the signal prediction from simulation as pink boxes. The red box indicates the region defined by the ZZ fiducial cuts on the Z candidate masses. The blue dashed lines indicate the regions where one of the leptons pairs is in the mass window $66 < m_{ll} < 116$ GeV. Contributions from events with one or both Z bosons outside of this mass window are also seen.

(lower p_{T}) lepton pair. Events are required to contain two Z candidates with invariant masses satisfying $66 < m_{\ell^+\ell^-} < 116$ GeV, resulting in 305 observed events.

4 Signal Acceptance

The ZZ selection requirements described above are applied to Monte Carlo simulation (PowHegBox and gg2zz), and corrections are applied to account for differences in lepton reconstruction and identification efficiency, lepton energy scale and resolution, and trigger efficiencies between data and simulation. The corrections are measured in data using samples of single $Z \to \ell^+\ell^-$ events, supplemented by samples of $J/\psi \to e^+e^-$ events for electron efficiency measurements at low p_{T}. The overall efficiency correction factor is 0.92±0.06 for the $e^+e^-e^+e^-$ channel, 0.97±0.03 for the $\mu^+\mu^-\mu^+\mu^-$ channel and 0.94±0.03 for the $e^+e^-\mu^+\mu^-$ channel, where the errors are systematic. A smearing and scale correction is added to the muon p_{T} in the simulation [38] so that the $Z \to \mu^+\mu^-$ invariant mass distribution in data is reproduced. Similarly, corrections are applied to the electron calorimeter energy resolution in the simulation and to the electron calorimeter energy scale in the data [39]. A correction parameterized by the number of

primary vertices in the event is applied to the calorimetric isolation of muons above $|\eta| = 2.5$ to account for the effects of pile-up.

The reconstruction acceptance factors, C_{ZZ}, used to correct from the observed events to the number of events in the ZZ fiducial phase-space, taking into account the experimental selection efficiencies and small contamination from ZZ decays involving τ leptons, are 0.55±0.04, 0.83±0.03 and 0.66±0.03 for the $e^+e^-e^+e^-$, $\mu^+\mu^-\mu^+\mu^-$ and $e^+e^-\mu^+\mu^-$ channel, respectively, where the errors are the combined statistical and systematic uncertainties. The lower signal efficiency in the $e^+e^-e^+e^-$ channel compared with the $\mu^+\mu^-\mu^+\mu^-$ channel reflects the lower electron identification efficiency. In all channels, the reconstruction acceptance has increased significantly with respect to a similar analysis on 7 TeV data collected in 2011, owing to improvements in the reconstruction algorithms. The dominant systematic uncertainties arise from the lepton identification and reconstruction efficiency and the efficiency of the isolation and impact parameter requirements. Uncertainties on the trigger efficiency, the lepton energy scale and resolution, and theoretical uncertainties from the PDFs and the choice of the renormalization and factorization scales, are small. The uncertainties are estimated by varying the data-driven correction factors applied to simulation by their systematic and statistical uncertainties. The theoretical uncertainties from the PDF, the factorization and renormalization scales and the MC generator are evaluated by taking the difference in C_{ZZ} obtained when using the CT10 and MSTW2008 PDF sets [40], when varying the factorization and renormalization scale by a factor of two, and when using Sherpa [41] as the MC generator, respectively.

The fiducial acceptance factor A_{ZZ}, used to correct from the number of observed events in the ZZ fiducial phase-space to the number of events in the total phase space, is calculated at NLO using MCFM version 6.3 with the CT10 PDF set and is determined to be 0.64±0.01. The error is due to the theoretical and statistical uncertainties. The theoretical uncertainties include the PDF uncertainty, evaluated by taking the difference between the A_{ZZ} obtained using the CT10 and MSTW2008 PDF sets and by determining the variation using the 52 CT10 error sets, and uncertainties in the factorization and renormalization scales, evaluated by moving each scale up and down by a factor of two. An additional uncertainty due to ISR, FSR and underlying event modelling is evaluated by comparing the acceptance in MCFM (where the effects of ISR, FSR and underlying event are not modelled) and PowhegBox (where they are). The total systematic uncertainty of the fiducial-to-total phase-space acceptance correction is found to be 1.3%. A summary of the systematic uncertainties on C_{ZZ} and A_{ZZ} is shown in Table 1.

5 Background Estimation

The main background to the ZZ signal originates from events with a Z (or $W^{\pm}$) boson decaying to leptons plus additional jets or photons (referred to as $W^{\pm}/Z + X$). Events with a top-quark pair, a single-top and other diboson processes (W^+W^-, $W^{\pm}Z$) also contribute. Jets may be misidentified as electrons or contain electrons and muons from in-flight decays of light mesons or heavy-flavoured hadrons which satisfy the electron or muon object selection. Photons may be misidentified as electrons. Leptons from heavy-flavour decays tend to be rejected by the impact parameter significance requirement. Leptons from misidentified jets or decays of light mesons tend to be spatially correlated with jets and many are rejected by the isolation requirement. Photons tend to be rejected due to hit requirements in the inner detector used in the electron identification. Since Monte Carlo simulations may not adequately describe the jet fragmentation in the tails of the isolation distributions, the background is estimated directly from the data.

To estimate the background contribution from four-lepton events in which at least one lepton candidate originates from a jet or a photon rather than from the decay of a Z boson, a control sample of events containing three leptons passing all selection criteria plus one *lepton-like jet* and two leptons passing all selection criteria plus two *lepton-like jets* are identified and denoted $\ell\ell\ell j$ and $\ell\ell jj$ respectively. For

Source	$e^+e^-e^+e^-$	$\mu^+\mu^-\mu^+\mu^-$	$e^+e^-\mu^+\mu^-$	$\ell^+\ell^-\ell'^+\ell'^-$
Reconstruction Uncertainties				
Lepton identification and reconstruction	6.2%	1.2%	3.1%	2.8%
Lepton energy/momentum	0.4%	<0.1%	0.2%	0.1%
Lepton isolation and impact parameter	1.8%	2.6%	1.5%	1.6%
Trigger efficiency	<0.1%	0.2%	0.1%	0.1%
Total Reconstruction Uncertainty (C_{ZZ})	6.4%	2.8%	3.4%	3.3%
Theoretical Uncertainties				
PDF & Scale (C_{ZZ})	0.1%	0.1%	<0.1%	<0.1%
MC Generator Difference (C_{ZZ})	1.7%	0.9%	1.8%	1.5%
PDF & Scale (A_{ZZ})	1.0%			
MC Generator Difference (A_{ZZ})	0.8%			
Total for C_{ZZ}	6.6%	3.0%	3.9%	3.6%
Total for A_{ZZ}	1.3%			
Luminosity	2.8%			

Table 1: Summary of systematic uncertainties, as relative percentages of the correction factor C_{ZZ} or the acceptance of the fiducial region A_{ZZ}. Sums in quadrature of the weighted average of the three channels and a combined *llll* uncertainty are shown for the reconstruction uncertainties. The assignment of the various uncertainties to the two correction factors (C_{ZZ}) and (A_{ZZ}) are shown in parenthesis next to the description of the uncertainty source.

	Selected leptons	Lepton-like jets
Muons	track isolation < 15% d_0-significance < 3.0	(d_0-significance > 3.0 and track isolation < 15%) or (d_0-significance < 3.0 and track isolation > 15%)
Electrons	track isolation < 15% and PASSES IDENTIFICATION ALGORITHM	(FAILS IDENTIFICATION ALGORITHM and track isolation < 15%) or (PASSES IDENTIFICATION ALGORITHM and track isolation > 15%)

Table 2: Summary of requirements for selected leptons and lepton-like jets. The full selection for electrons and muons is applied to the selected leptons and lepton-like jets with the exception of those listed in the table.

muons, the lepton-like jets are muon candidates that either fail the track isolation requirement but pass the d_0 significance requirement or fail the d_0 significance requirement but pass the track isolation requirement. For muons with $|\eta| > 2.5$, calorimetric isolation is used instead of track isolation. For electrons, the lepton-like jets are energy deposits in the electromagnetic calorimeter matched to inner detector tracks that either fail the electron identification requirement [39] but pass the track isolation requirement, or fail the track isolation requirement but pass the electron identification requirement. The events are otherwise required to pass the full event selection, treating the lepton-like jet as if it were an identified lepton. The definitions of lepton-like jets are summarized in Table 2.

Since the selected leptons are spatially separated in ΔR because of the isolation requirements, we require that the lepton-like jets do not overlap with another lepton-like jet or selected lepton within a cone of $\Delta R = 0.2$. This ensures that the control sample has similar kinematic characteristics to the signal sample. This event sample is dominated by $Z+X$ events for the $e^+e^-e^+e^-$ channel and $Z+X$ and $t\bar{t}$ events for the $e^+e^-\mu^+\mu^-$ and $\mu^+\mu^-\mu^+\mu^-$ channels.

The background is then estimated by scaling the control sample by a measured 'fake factor' f (η and p_{T} dependent, treated as uncorrelated in the two variables) which is the ratio of the probability for 'background' leptons to satisfy the lepton criteria to the probability to satisfy the lepton-like jet criteria, where 'background' leptons are leptons from jets or photons as described above. The background in which two of the selected leptons originate from a jet or photon is treated similarly, using the $\ell\ell jj$ sample. A correction is necessary to account for the number of ZZ signal events which decay to four leptons where three leptons pass the selected lepton requirements and one passes the lepton-like jet requirements ($N_{ZZ}^{\ell\ell\ell j}$), or two leptons pass the selected lepton requirements and two pass the lepton-like jet requirements ($N_{ZZ}^{\ell\ell jj}$). This is estimated using signal Monte Carlo expectation. The background from events with misidentified (fake) leptons is calculated as:

$$N_{4\ell}^{\mathrm{fake}} = N(\ell\ell\ell j) \times f - N(\ell\ell jj) \times f^2 - N_{ZZ}^{Correction} \tag{1}$$

where $N_{ZZ}^{Correction} = N_{ZZ}^{\ell\ell\ell j} \times f - N_{ZZ}^{\ell\ell jj} \times f^2$. The factor f is measured in a sample of data selected by requiring a reconstructed opposite-sign same-flavour lepton pair which has an invariant mass within 20 GeV of the Z mass and classifying any additional identified leptons in the event as selected leptons or lepton-like jets. It is assumed that all of these additional leptons are 'fakes', either from light jets misidentified as real leptons, bremsstrahlung photons converting to electrons, or from real leptons from decays in heavy flavour jets. Contributions to f from $W^{\pm}Z$ and ZZ processes, which contain additional real leptons, are subtracted from the data using simulation, normalized using the SM cross sections. The systematic uncertainty is determined by comparing the nominal data-driven background estimation using the parameterized fake factor (in η and p_T) and the estimation using the average fake factor (total ℓ divided by total j) for each type of lepton. The difference is the systematic quoted in Table 3.

Ingredients in Eq.1	$e^+e^-e^+e^-$	$\mu^+\mu^-\mu^+\mu^-$	$e^+e^-\mu^+\mu^-$	$\ell^+\ell^-\ell'^+\ell'^-$
$N(\ell\ell\ell j)$	164	7	117	288
(+) $N(\ell\ell\ell j) \times f$	21.7 ± 1.7	3.3 ± 1.3	20.1 ± 2.0	45.1 ± 2.8
$N(\ell\ell jj)$	646	9	453	1108
(−) $N(\ell\ell jj) \times f^2$	11.0 ± 0.4	1.0 ± 0.4	8.4 ± 0.4	20.5 ± 0.6
(−) $N_{ZZ}^{Correction}$	1.1 ± 0.1	1.7 ± 0.4	3.1 ± 0.4	5.9 ± 0.5
Background, $N_{4\ell}^{\text{fake}}$	9.6±1.8 ± 1.4	0.6 ± 1.4 ± 0.5	8.5 ± 2.1 ± 3.1	18.7 ± 2.9 ± 5.0
MC, irreducible	0.4±0.1	0.5±0.1	0.7±0.1	1.6±0.1
Total background	10.0±1.8±1.4	1.1±1.4±0.5	9.3±2.1±3.1	20.4±2.9±5.0

Table 3: Components of the ZZ background estimate. The first row gives the number of observed events with three selected leptons and one lepton-like jet. The second row gives this number multiplied by the factor f. Similarly the third row gives the number of observed events with two selected leptons and two lepton-like jets, and the fourth gives this number multiplied by the factor f^2. The fifth row gives the correction due to ZZ events. Only statistical errors are given for these quantities. Lines two, four and five are combined using Equation 1 to give the background estimate from fake sources, which is shown in the sixth row. The irreducible backgrounds estimated from Monte Carlo are shown in the seventh row while the total background estimate is shown in the last row. The first uncertainty is statistical while the second is systematic.

Sources of irreducible background such as $t\bar{t}Z$, ZZZ and ZWW must also be taken into consideration when calculating the background estimation. The contribution from these sources is estimated from Monte Carlo and added to the data-driven estimation to give the total background expectation. Table 3 shows the observed values for the components of Equation 1, as well as the final background estimate. The statistical uncertainty on the background estimate is the combination of $N(\ell\ell\ell j)$, $N(\ell\ell jj)$ and the $N_{ZZ}^{Correction}$, while the systematic uncertainty comes from the data-driven background systematic described above.

6 Cross Section Measurement

The numbers of expected and observed events after applying all selection criteria are shown in Table 4, along with the reconstruction acceptance factors used to correct back to the number of events in the fiducial phase-space, taking into account the contribution from events where at least one of the Z bosons decays to τ leptons. We observe 305 candidates passing the ZZ selection in data, with a background expectation of 20.4±2.9(stat)±5.0(syst.).

Figure 3 shows the invariant mass distributions for the leading and subleading lepton pairs after all selection requirements are applied, the transverse momentum distributions of the lepton pairs and the four-lepton system, and the invariant mass of the four-lepton system. The distributions for each decay channel can be found in Appendix A, Figures 5, 6 and 7. No significant discrepancy is observed between the data and the expectations.

The ZZ cross sections are determined using a likelihood fit with the systematic uncertainties included as nuisance parameters. The final result for the fiducial cross section corresponding to the phase-space

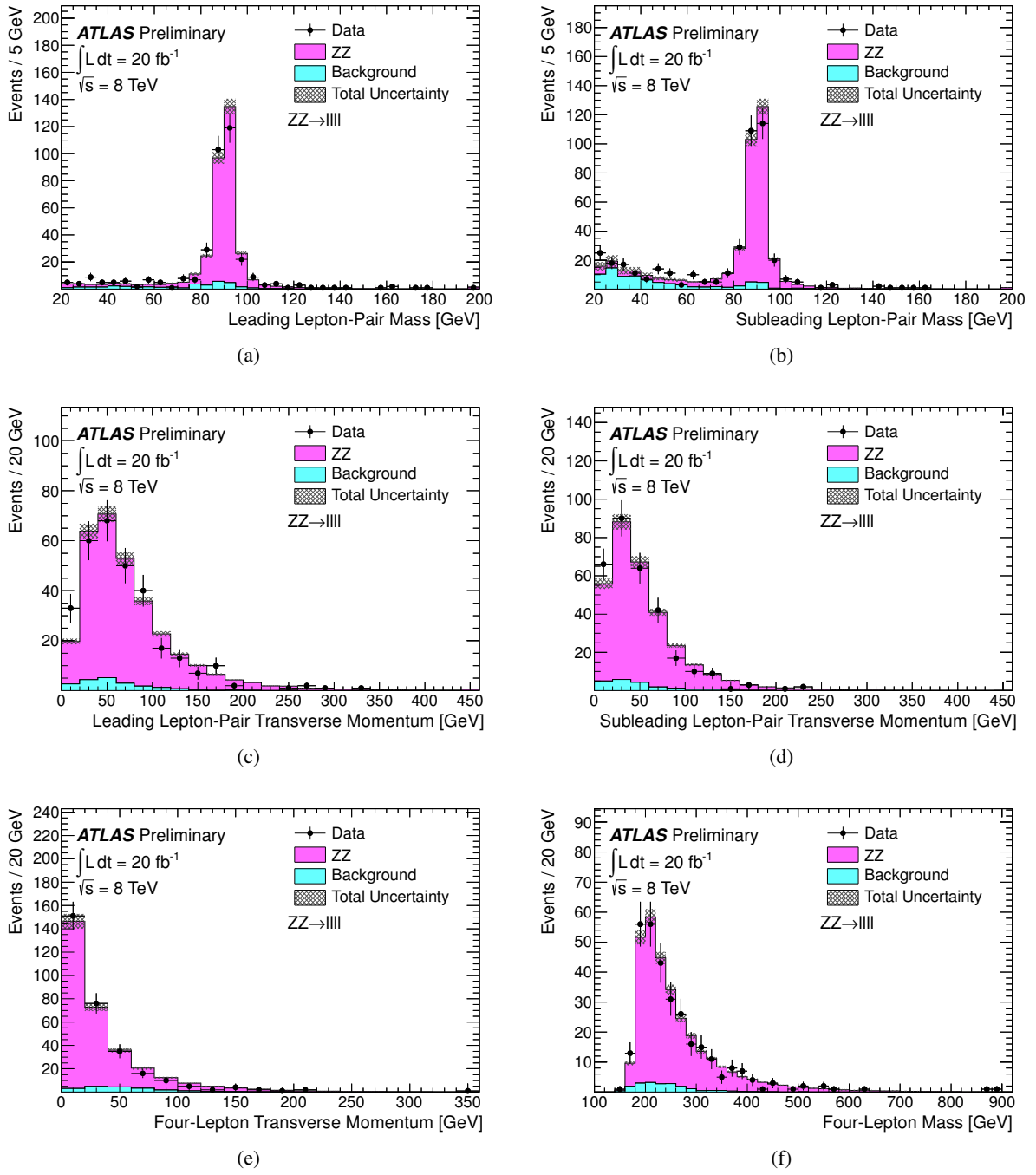

Figure 3: Kinematic distributions for ZZ candidates in all four-lepton channels. The dilepton mass distribution is shown in (a) for the leading pair and (b) for the subleading pair. The full event selection criteria are applied except for the dilepton mass requirement on the distribution being plotted. For the plots shown in (c), (d), (e) and (f), the full event selection is applied. The dilepton transverse momentum is shown in (c) for the leading pair and (d) for the subleading pair. Finally the four-lepton transverse momentum and invariant mass distributions are shown in (e) and (f), respectively. In all figures, the points are data and the stacked histograms show the signal and background predictions from simulation. The signal is normalized to the integrated luminosity of the data. The background distributions are normalized to the total background estimate. The grey band indicates the combined statistical and systematic uncertainty on the signal and background predictions.

Final state	$e^+e^-e^+e^-$	$\mu^+\mu^-\mu^+\mu^-$	$e^+e^-\mu^+\mu^-$	$\ell^+\ell^-\ell'^+\ell'^-$
Observed	62	85	158	305
Signal (MC)	59.5±4.0	90.2±2.7	142.7±5.6	292.5±10.6
Background	10.0±1.8±1.4	1.1±1.4±0.5	9.3±2.1±3.1	20.4±2.9±5.0
C_{ZZ}	0.55±0.04	0.83±0.03	0.66±0.03	0.68±0.02

Table 4: Summary of observed events, expected signal and background contributions, and reconstruction acceptance factor in all four-lepton channels, after applying the ZZ selection. The signal expectation is derived from Monte Carlo and is shown with the combined statistical and systematic uncertainty. The luminosity uncertainty on the signal expectation is 2.8%. The background predictions are obtained as discussed in Sec. 5. The first error is statistical while the second is systematic. The reconstruction acceptance factor, C_{ZZ}, is estimated from Monte Carlo as discussed in Sec. 4 and is shown with its combined statistical and systematic uncertainty.

defined in Section 1 is:

$$\sigma^{\rm fid}_{ZZ\to\ell^-\ell^+\ell'^-\ell'^+} = 20.7^{+1.3}_{-1.2}(\text{stat.}) \pm 0.8(\text{syst.}) \pm 0.6(\text{lumi.})\ \text{fb}$$

where $\ell^+\ell^-\ell'^+\ell'^-$ refers to the sum of the $e^+e^-e^+e^-$, $\mu^+\mu^-\mu^+\mu^-$ and $e^+e^-\mu^+\mu^-$ final states. This result is consistent with the Standard Model prediction of $21.1^{+0.9}_{-0.7}$ fb, calculated at NLO using MCFM, where the error reflects the uncertainty on the PDFs and on the scales, as described below. The fiducial cross sections in each decay channel are shown in Table 5.

Channel	Measured σ_{fid} [fb]	Theoretical σ_{fid} [fb]
$ZZ \to e^+e^-e^+e^-$	$4.6^{+0.8}_{-0.7}(\text{stat.})^{+0.4}_{-0.4}(\text{syst.})^{+0.1}_{-0.1}(\text{lumi.})$	$5.3^{+0.2}_{-0.2}$
$ZZ \to \mu^+\mu^-\mu^+\mu^-$	$5.0^{+0.6}_{-0.5}(\text{stat.})^{+0.2}_{-0.2}(\text{syst.})^{+0.2}_{-0.2}(\text{lumi.})$	$5.3^{+0.2}_{-0.2}$
$ZZ \to e^+e^-\mu^+\mu^-$	$11.1^{+1.0}_{-0.9}(\text{stat.})^{+0.5}_{-0.5}(\text{syst.})^{+0.3}_{-0.3}(\text{lumi.})$	$10.5^{+0.4}_{-0.4}$

Table 5: Fiducial cross sections per channel. The measured value is compared to the theoretical prediction from MCFM.

The total cross section is determined by extrapolating the ZZ fiducial cross section to the full phase-space, correcting for the $Z \to \ell^+\ell^-$ branching ratio and the acceptance of the fiducial cuts. The measured value of the total ZZ cross section is:

$$\sigma^{\rm tot}_{ZZ} = 7.1^{+0.5}_{-0.4}(\text{stat.}) \pm 0.3(\text{syst.}) \pm 0.2(\text{lumi.})\ \text{pb}.$$

This result is consistent with the Standard Model prediction of $7.2^{+0.3}_{-0.2}$ pb, calculated at NLO using MCFM and the CT10 PDF set.

Figure 4 shows measurements of the total ZZ production cross section as a function of centre-of-mass energy, showing results from the ATLAS [5] and CMS [6, 8] experiments at the LHC, and from the CDF [14] and D0 [15] experiments at the Tevatron, as well as the theoretical predictions.

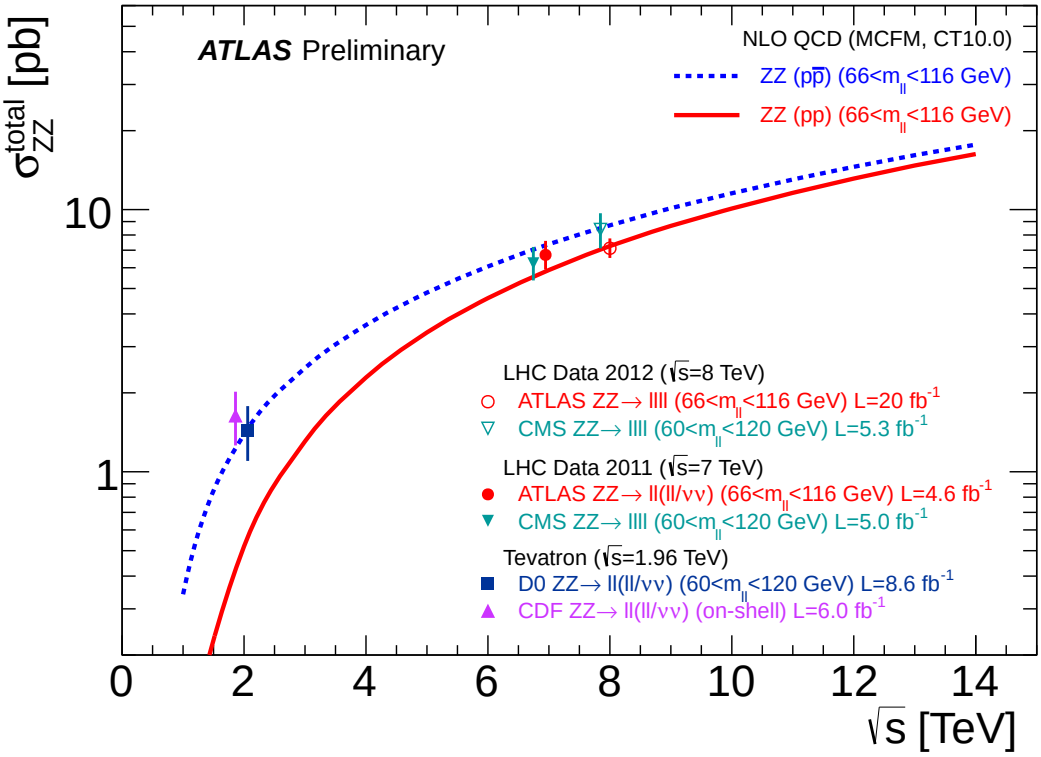

Figure 4: Comparison of experimental measurements and theoretical predictions of the total ZZ production cross section as a function of centre-of-mass energy $\sqrt{s}$. Shown are experimental measurements from CDF [14] and D0 [15] in $p\bar{p}$ collisions at the Tevatron at $\sqrt{s} = 1.96$ TeV, and experimental measurements from ATLAS [5] and CMS [6, 8] in pp collisions at the LHC at $\sqrt{s} = 7$ TeV and $\sqrt{s} = 8$ TeV. The blue dashed line shows the theoretical prediction for the ZZ production cross section in $p\bar{p}$ collisions, calculated at NLO in QCD using MCFM with PDF set CT10. The solid red line shows the theoretical prediction for the ZZ production cross section in pp collisions, calculated in the same way. The theoretical curves are calculated using the natural width of the Z boson in the mass range 66 to 116 GeV. At $\sqrt{s} = 8$ TeV, the theoretical prediction using the zero-width approximation is 5% higher than the prediction using the natural width, restricted to the mass range 66 to 116 GeV.

7 Conclusions

A measurement of the ZZ production cross section in LHC proton-proton collisions at $\sqrt{s}$ = 8 TeV has been performed using data collected by the ATLAS detector in 2012, with electrons and muons in the final state. The dataset corresponds to an integrated luminosity of 20.3±0.6 fb^{-1}. In total, 305 candidate ZZ events with both lepton pairs in the mass range $66 < m_{\ell^+\ell^-} < 116$ GeV are observed, with a background expectation of 20.4±2.9(stat)±5.0(syst.). The Standard Model expectation for the number of signal events is 292.5±10.6. The fiducial and total ZZ production cross sections are determined to be:

$$\begin{aligned} \sigma^{\text{fid}}_{ZZ\to\ell^-\ell^+\ell'^-\ell'^+} &= 20.7^{+1.3}_{-1.2}(\text{stat.}) \pm 0.8(\text{syst.}) \pm 0.6(\text{lumi.})\ \text{fb} \\ \sigma^{\text{tot}}_{ZZ} &= 7.1^{+0.5}_{-0.4}(\text{stat.}) \pm 0.3(\text{syst.}) \pm 0.2(\text{lumi.})\ \text{pb} \end{aligned}$$

where the fiducial cross section is defined with both Z bosons with mass between 66 GeV and 116 GeV, all four leptons with $p_{\text{T}} > 7$ GeV, $|\eta| < 2.7$ and no pair of leptons with $\Delta R < 0.2$, while the total cross section is defined with both Z bosons with mass between 66 GeV and 116 GeV. The results are in good agreement with the NLO Standard Model total cross section for this process of $7.2^{+0.3}_{-0.2}$ pb and supercede the previous measurements made with part of the same dataset [7].

References

[1] J. Campbell, K. Ellis, and C. Williams, *Vector boson pair production at the LHC*, JHEP **1107** (2011) 018, arXiv:1105.0020 [hep-ph].

[2] G. J. Gounaris, J. Layssac, and F. M. Renard, *Off-shell structure of the anomalous Z and γ self-couplings*, Phys. Rev. **D62** (2000) 073012, arXiv:hep-ph/0005269.

[3] J. Ellison and J. Wudka, *Study of trilinear gauge boson couplings at the Tevatron Collider*, Annu. Rev. Nucl. Part. Sci. **48** (1998) 33, arXiv:hep-ph/9804322.

[4] U. Baur and D. L. Rainwater, *Probing neutral gauge boson self interactions in ZZ production at hadron colliders*, Phys. Rev. **D62** (2000) 113011, arXiv:hep-ph/0008063.

[5] ATLAS Collaboration, *Measurement of ZZ production in pp collisions at $\sqrt{s} = 7$ TeV and limits on anomalous ZZZ and ZZγ couplings with the ATLAS detector*, arXiv:1211.6096 [hep-ex].

[6] CMS Collaboration, *Measurement of the ZZ production cross section and search for anomalous couplings in $2\ell 2\ell'$ final states in pp collisions at $\sqrt{s} = 7$ TeV*, JHEP **1301** (2013) 063, arXiv:1211.4890 [hep-ex].

[7] ATLAS Collaboration, *Measurement of the total ZZ production cross section in the four-lepton channel using 5.8 fb^{-1} of ATLAS data at $\sqrt{s} = 8$ TeV*, ATLAS-CONF-2012-090 . http://cdsweb.cern.ch/record/1460409.

[8] CMS Collaboration, *Measurement of W^+W^- and ZZ production cross sections in pp collisions at $\sqrt{s} = 8$ TeV*, arXiv:1301.4698 [hep-ex].

[9] ALEPH Collaboration, R. Barate et al., *Measurement of the $e^+e^- \to Z\,Z$ production cross section at centre-of-mass energies of 183 GeV and 189 GeV*, Phys. Lett. **B469** (1999) 287, arXiv:hep-ex/9911003.

[10] DELPHI Collaboration, J. Abdallah et al., *ZZ production in e^+e^- interactions at $\sqrt{s}$ = 183 GeV to 209 GeV*, Eur. Phys. J. **C30** (2003) 447, arXiv:hep-ex/0307050.

[11] L3 Collaboration, M. Acciarri et al., *Study of Z boson pair production in e^+e^- collisions at LEP at $\sqrt{s}$ = 189 GeV*, Phys. Lett. **B465** (1999) 363, arXiv:hep-ex/9909043.

[12] OPAL Collaboration, G. Abbiendi et al., *Study of Z pair production and anomalous couplings in e^+e^- collisions at $\sqrt{s}$ between 190 GeV and 209 GeV*, Eur. Phys. J. **C32** (2003) 303, arXiv:hep-ex/0310013.

[13] The LEP Collaborations ALEPH, DELPHI, L3, OPAL, and the LEP Electroweak Working Group, *A Combination of preliminary electroweak measurements and constraints on the Standard Model*, arXiv:hep-ex/0612034.

[14] CDF Collaboration, T. Aaltonen et al., *Measurement of ZZ production in leptonic final states at $\sqrt{s}$ of 1.96 TeV at CDF*, Phys. Rev. Lett. **108** (2012) 101801, arXiv:1112.2978 [hep-ex].

[15] D0 Collaboration, V. M. Abazov et al., *A measurement of the WZ and ZZ production cross sections using leptonic final states in 8.6 fb^{-1} of $p\bar{p}$ collisions*, Phys. Rev. **D85** (2012) 112005, arXiv:1201.5652 [hep-ex].

[16] H.-L. Lai et al., *New parton distributions for collider physics*, Phys. Rev. **D82** (2010) 074024, arXiv:1007.2241 [hep-ph].

[17] J. Beringer et al. (Particle Data Group), *The review of particle physics*, Phys. Rev. **D86** (2012) 010001.

[18] ATLAS Collaboration, *ATLAS experiment at the CERN Large Hadron Collider*, JINST **3** (2008) S08003.

[19] ATLAS Collaboration, *Improved luminosity determination in pp collisions at* $\sqrt{s} = 7$ *TeV using the ATLAS detector at the LHC*, arXiv:1302.4393 [hep-ex].

[20] T. Melia, P. Nason, R. Rontsch, and G. Zanderighi, W^+W^-*, WZ and ZZ production in the POWHEG BOX*, JHEP **1111** (2011) 078, arXiv:1107.5051 [hep-ph].

[21] S. Alioli, P. Nason, C. Oleari, and E. Re, *A general framework for implementing NLO calculations in shower Monte Carlo programs: the POWHEG BOX*, JHEP **1006** (2010) 043, arXiv:1002.2581 [hep-ph].

[22] S. Frixione, P. Nason, and C. Oleari, *Matching NLO QCD computations with Parton Shower simulations: the POWHEG method*, JHEP **0711** (2007) 070, arXiv:0709.2092 [hep-ph].

[23] P. Nason, *A New method for combining NLO QCD with shower Monte Carlo algorithms*, JHEP **0411** (2004) 040, arXiv:hep-ph/0409146.

[24] T. Binoth, N. Kauer, and P. Mertsch, *Gluon-induced QCD corrections to* $pp \to ZZ \to \ell^+\ell^-\ell'^+\ell'^-$, arXiv:0807.0024 [hep-ph].

[25] S. Frixione and B.R. Webber, *Matching NLO QCD computations and parton shower simulations*, JHEP **0206** (2002) 029.

[26] J. Alwall et al., *MadGraph/MadEvent v4: the new web generation*, JHEP **0709** (2007) 028, arXiv:0706.2334 [hep-ph].

[27] S. P. Baranov and M. Smižanská, *Semihard b quark production at high-energies versus data and other approaches*, Phys. Rev. **D62** (2000) 014012.

[28] T. Sjostrand, S. Mrenna, and P. Skands, *A brief introduction to PYTHIA 8.1*, Comput. Phys. Commun. **178** (2008) 852, arXiv:0710.3820 [hep-ph].

[29] J. Butterworth, J. Forshaw, and M. Seymour, *Multiparton interactions in photoproduction at HERA*, Z. Phys. **C72** (1996) 637, arXiv:hep-ph/9601371.

[30] G. Corcella et al., *HERWIG 6.5: an event generator for Hadron Emission Reactions With Interfering Gluons (including supersymmetric processes)*, JHEP **0101** (2001) 010, arXiv:hep-ph/0011363.

[31] S. Jadach, J. H. Kühn, and Z. Was, *TAUOLA - a library of Monte Carlo programs to simulate decays of polarized* τ *leptons*, Comput. Phys. Commun. **64** (1991) 275.

[32] P. Golonka and Z. Was, *PHOTOS Monte Carlo: a precision tool for QED corrections in Z and W decays*, Eur. Phys. J. **C45** (2006) 97, arXiv:hep-ph/0506026.

[33] ATLAS Collaboration, *ATLAS simulation infrastructure*, Eur. Phys. J. **C70** (2010) 823.

[34] S. Agostinelli et al., *Geant4 – a simulation Toolkit*, Nucl. Instrum. Meth. **A506** (2003) 250.

[35] R. Fruhwirth, *Track fitting with non-Gaussian noise*, Comput. Phys. Commun. **100** (1997) no. 1-2, 1.

[36] ATLAS Collaboration, *Improved electron reconstruction in ATLAS using the Gaussian Sum Filter-based model for bremsstrahlung*, ATLAS-CONF-2012-047 . http://cdsweb.cern.ch/record/1449796.

[37] ATLAS Collaboration, *Observation of a new particle in the search for the Standard Model Higgs boson with the ATLAS detector at the LHC*, Phys. Lett. **B716** (2012) 1–29, arXiv:1207.7214 [hep-ex].

[38] ATLAS Collaboration, *ATLAS muon momentum resolution in the first pass reconstruction of the 2010 p-p collision data at* $\sqrt{s}$ *= 7 TeV*, ATLAS-CONF-2011-046 . http://cdsweb.cern.ch/record/1338575.

[39] ATLAS Collaboration, *Electron performance measurements with the ATLAS detector using the 2010 LHC proton-proton collision data*, Eur. Phys. J. **C72** (2012) 1909, arXiv:1110.3174 [hep-ex].

[40] A. D. Martin, W. J. Stirling, R. S. Thorne, and G. Watt, *Parton distributions for the LHC*, Eur. Phys. J. **C63** (2009) 189, arXiv:0901.0002 [hep-ph].

[41] T. Gleisberg et al., *Event generation with Sherpa 1.1*, JHEP **0902** (2009) 007, arXiv:0811.4622 [hep-ph], http://projects.hepforge.org/sherpa/doc/SHERPA-MC-1.3.1.html.

A $ZZ \to \ell^-\ell^+\ell'^-\ell'^+$ Kinematic distributions per channel

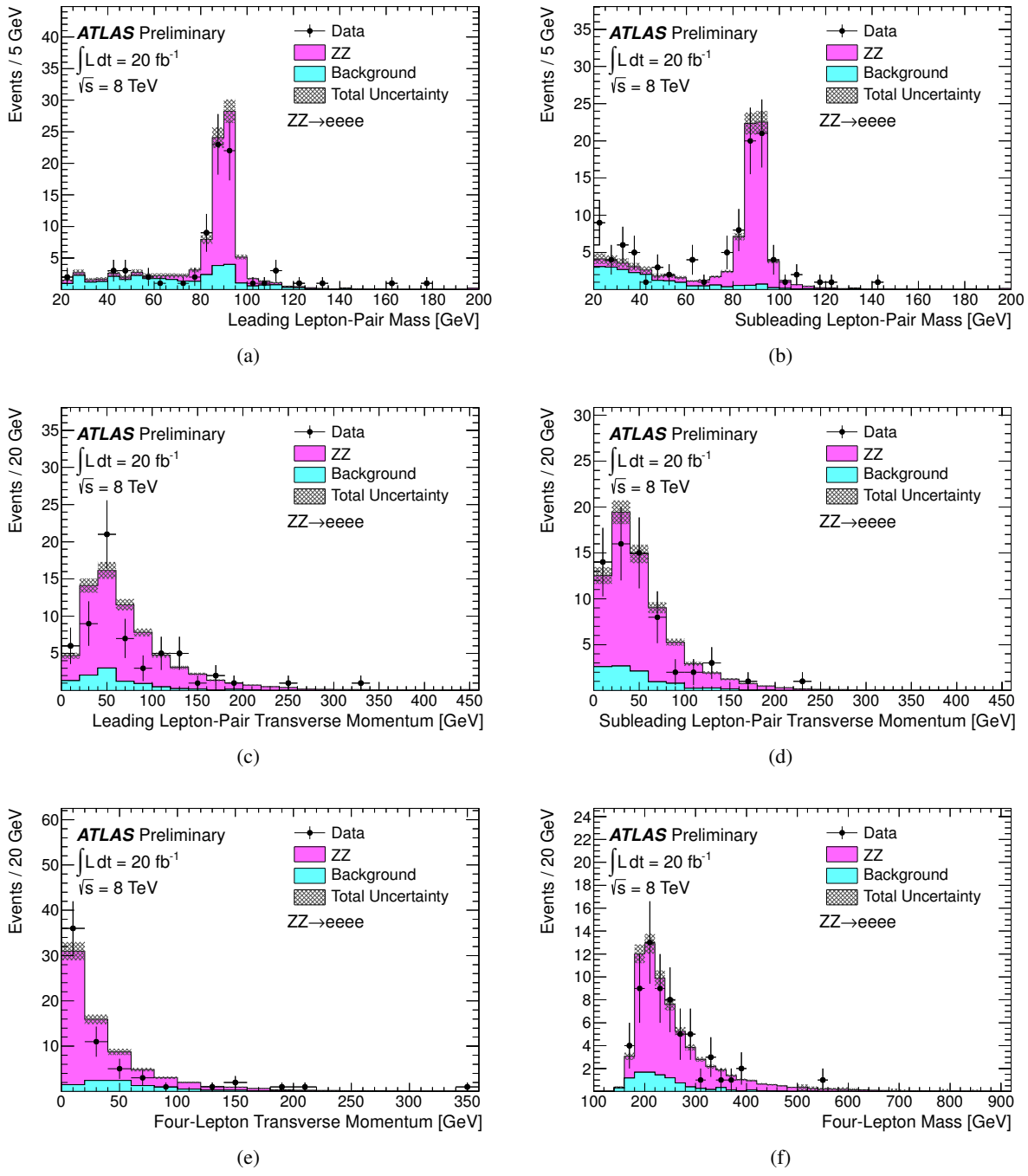

Figure 5: Kinematic distributions for ZZ candidates in the four-electron channel. The dilepton mass distribution is shown in (a) for the leading pair and (b) for the subleading pair. The full event selection criteria are applied except for the dilepton mass requirement on the distribution being plotted. For the plots shown in (c), (d), (e) and (f), the full event selection is applied. The dilepton transverse momentum is shown in (c) for the leading pair and (d) for the subleading pair. Finally the four-lepton transverse momentum and invariant mass distributions are shown in (e) and (f), respectively. In all figures, the points are data and the stacked histograms show the signal and background predictions from simulation. The signal is normalized to the integrated luminosity of the data. The background distributions are normalized to the total background estimate. The grey band indicates the combined statistical and systematic uncertainty on the signal and background predictions.

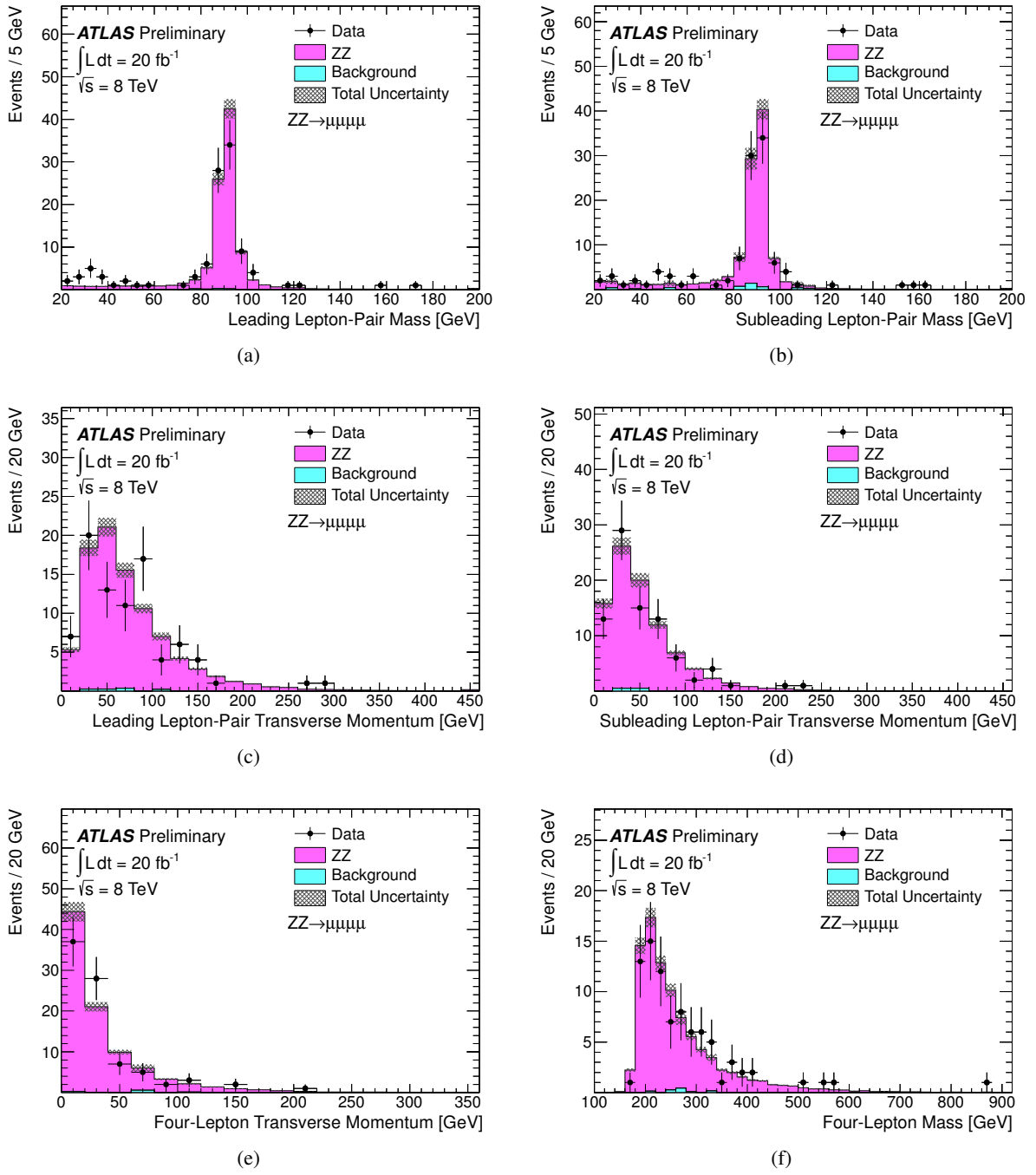

Figure 6: Kinematic distributions for ZZ candidates in the four-muon channel. The dilepton mass distribution is shown in (a) for the leading pair and (b) for the subleading pair. The full event selection criteria are applied except for the dilepton mass requirement on the distribution being plotted. For the plots shown in (c), (d), (e) and (f), the full event selection is applied. The dilepton transverse momentum is shown in (c) for the leading pair and (d) for the subleading pair. Finally the four-lepton transverse momentum and invariant mass distributions are shown in (e) and (f), respectively. In all figures, the points are data and the stacked histograms show the signal and background predictions from simulation. The signal is normalized to the integrated luminosity of the data. The background distributions are normalized to the total background estimate. The grey band indicates the combined statistical and systematic uncertainty on the signal and background predictions.

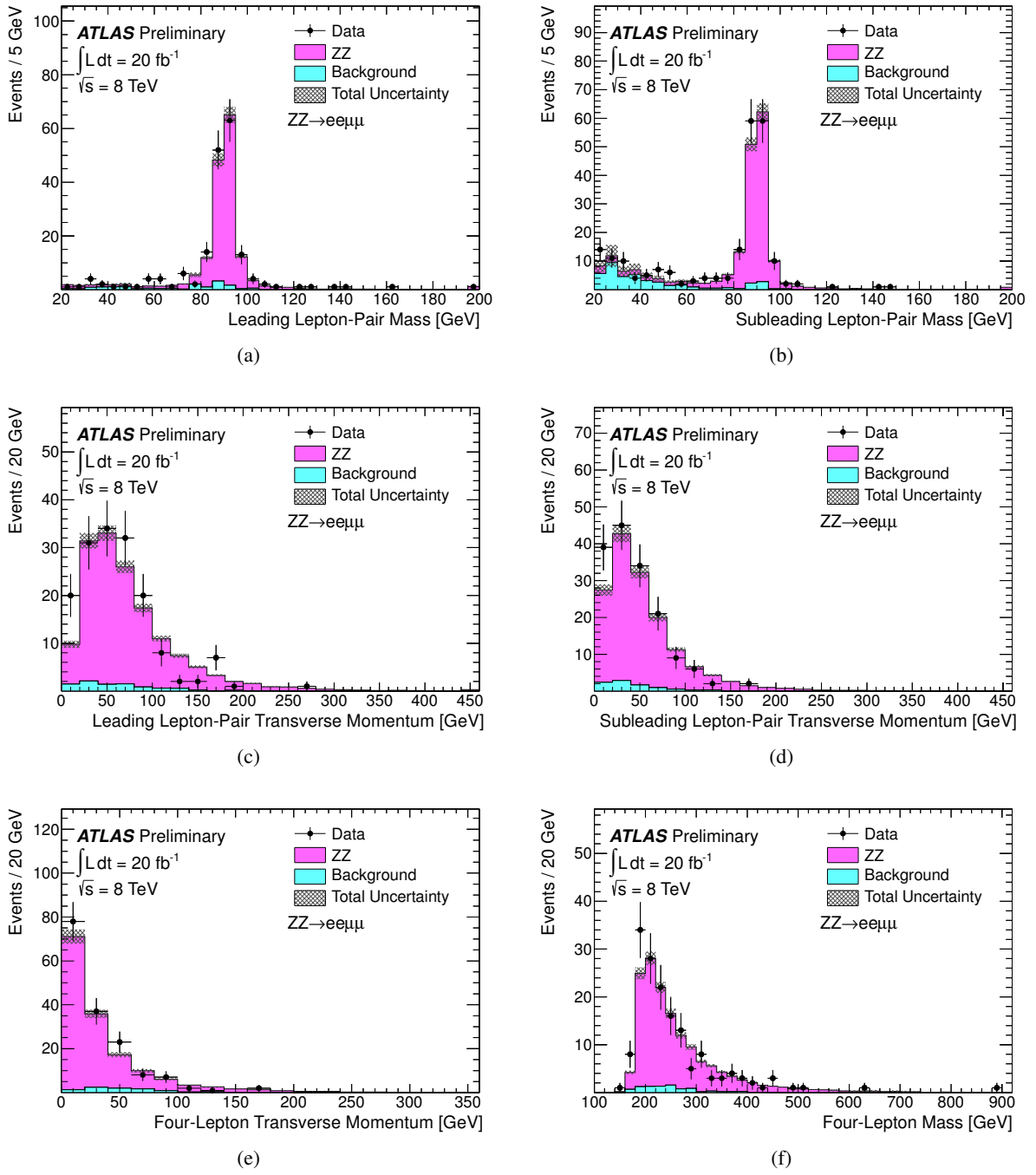

Figure 7: Kinematic distributions for ZZ candidates in the two-electron, two-muon channel. The dilepton mass distribution is shown in (a) for the leading pair and (b) for the subleading pair. The full event selection criteria are applied except for the dilepton mass requirement on the distribution being plotted. For the plots shown in (c), (d), (e) and (f), the full event selection is applied. The dilepton transverse momentum is shown in (c) for the leading pair and (d) for the subleading pair. Finally the four-lepton transverse momentum and invariant mass distributions are shown in (e) and (f), respectively. In all figures, the points are data and the stacked histograms show the signal and background predictions from simulation. The signal is normalized to the integrated luminosity of the data. The background distributions are normalized to the total background estimate. The grey band indicates the combined statistical and systematic uncertainty on the signal and background predictions.